Lipid−Peptide Interface: Valine Conformation and Dynamics in the Gramicidin Channel†

K.-C. Lee, S. Huo, and T. A. Cross*

Department of Chemistry & National High Magnetic Field Laboratory, Florida State University, Tallahassee, Florida 32306-3016

Received July 6, 1994; Revised Manuscript Received November 3, 1994®

ABSTRACT: High-resolution dynamic and structural characterizations have been achieved for each of the valine side chains of the gramicidin channel while solubilized in hydrated lipid bilayers. The characterizations have been achieved by ^2H NMR spectra of both oriented and unoriented samples obtained at 36 and 5 °C, respectively. Powder patterns displaying intermediate time frame averaging provide dynamic information, and quadrupole splittings from aligned samples provide orientational constraints for the side chain structure. Librational amplitudes for each site throughout the side chain have also been characterized. Val_6 and Val_8 are shown to be fixed in rotameric states, potentially constraining two of the indole rings and the functionally important indole dipole moment orientations. Val_1 and Val_7 undergo three-state jump motions. The jump frequencies increase from the microsecond to nanosecond time frame upon increasing the temperature through the lipid phase transition. For the same temperature range, there is no evidence for changes in conformational state populations. Despite small differences in the substate populations for the two residues, the motions may be loosely coupled as indicated by the high-resolution structure.

The lipid−protein interface has long been studied from the lipid side of this surface. The detailed characterization of the eight valine residues in the gramicidin channel dimer provides a unique glimpse into this interface near the bilayer center. The polypeptide backbone structure and dynamics have been well characterized in a lipid bilayer environment (Ketchem et al., 1993; North & Cross, 1993; Lazo et al., 1993). For the valine residues, the opportunity for large amplitude dynamics is restricted to a single torsion angle, χ_1. The determination of the χ_1 value or values for each residue and the determination of conformer populations represent a detailed characterization of both structure and dynamics for each residue. In light of the fluid nature of the lipid environment in the bilayer center, it is surprising that only two residues in each monomer show large amplitude side chain dynamics, Val_1 and Val_7. Leu_4, Val_6, and Val_8 are each confined to a single conformational state.

Gramicidin A has a sequence of alternating L- and D-amino acid residues:

HCO-(L)Val_1-Gly_2-(L)Ala_3-(D)Leu_4-(L)Ala_5-(D)Val_6-
(L)Val_7-(D)Val_8-(L)Trp_9-(D)Leu_{10}-(L)Trp_{11}-(D)Leu_{12}-
(L)Trp_{13}-(D)Leu_{14}-(L)Trp_{15}-NHC_2H_4OH

As a symmetric dimer, this polypeptide forms a monovalent cation-selective channel across lipid bilayers. The conductance has been well-characterized for a wide range of cations and modified sequences. With this simple channel there is an opportunity to derive unique structure−dynamic function correlations once the high-resolution structural and dynamic information is available.

The polypeptide fold is a β-strand with all side chains on one side, resulting from the D/L alternating sequence. This motif, which forms a helix having 6.3 residues per turn, was first proposed by Urry (1971) on the basis of modeling efforts. More recently, a solution NMR[1] structure in detergent micelles was achieved by ^1H homonuclear spectroscopy (Bystrov et al., 1987; Lomize et al., 1992) that confirmed the fold, with the exception that the structure was right-handed and not left-handed as characterized by Urry et al. (1982). While the channel conformation has not been characterized by X-ray crystallography, the three-dimensional structure of this conformation has been achieved in a lipid bilayer environment based on solid state NMR-derived orientational constraints (Ketchem et al., 1993). This structure confirmed the handedness determination by solution NMR methods and generated a very high-resolution (±3° in torsion angle rmsd) structure. It has been developed solely with data that constrain the orientation of specific nuclear sites with respect to a common axis, the magnetic field direction. To develop such orientational constraints, samples were uniformly aligned (Cross et al., 1992) with respect to the magnetic field. For samples of gramicidin in aligned lipid bilayers, the channel axis and bilayer normal are aligned parallel with the magnetic field. The primary orientation dependent nuclear spin interactions that have been used to develop the backbone structure are the ^{15}N chemical shift (Fields et al., 1988) and $^{15}N-^1H$ (LoGrasso et al., 1989) and $^{15}N-^{13}C$ dipolar (Teng et al., 1991) interactions. Numerous

† S.H. gratefully acknowledges support from the National High Magnetic Field Laboratory and T.A.C. gratefully acknowledges the National Institutes of Health for support through Grant AI23007.

® Abstract published in *Advance ACS Abstracts,* January 1, 1995.

[1] Abbreviations: NMR, nuclear magnetic resonance; HPLC, high-performance liquid chromatography; PAS, principal axis system; EFG, electric field gradient; QCC, quadrupole coupling constant; DMPC, dimyristoylphosphatidylcholine; DDW, deuterium-depleted water; Fmoc, 9-fluorenylmethoxycarbonyl; rmsd, root mean square deviation.

0006-2960/95/0434-857$09.00/0

solid state NMR research groups have contributed to the data base of orientational constraints for gramicidin [e.g., Koeppe et al. (1994), Hing et al. (1990), Separovic et al. (1993), and Prosser et al. (1994)]. Similar constraints have been used in other macromolecular systems (Ulrich et al., 1994; Bechinger et al., 1993; Yeo et al., 1994; Nicholson et al., 1993), and this approach has recently been reviewed (Cross, 1994; Cross & Opella, 1994).

Gramicidin dynamics have been studied extensively by computational and experimental methods. In fact, the molecule represents a unique opportunity for the comparison of results from these two approaches. With the addition of water and lipid to the computational systems, significant efforts are underway to characterize backbone (Woolf & Roux, 1994; Chiu et al., 1991) and side chain (Woolf & Roux, 1994; Woolf et al., 1993) dynamics. Experimentally, the backbone dynamics have been characterized by a range of solid state NMR methods (Nicholson et al., 1991; Separovic et al., 1993; Prosser & Davis, 1994; Lazo et al., 1993; North & Cross, 1993). Less data are available on side chain dynamics. The Val_1 dynamics have been debated in the literature (Killian et al., 1992; Lee & Cross, 1994). A detailed librational characterization of the indole rings and leucine side chains has recently been abstracted (Huo et al., 1994).

The indole rings have been shown to play multiple important roles for the gramicidin channel. The indole NH protons are all oriented toward the bilayer surface, presumably to hydrogen bond to the bilayer surface. It is known through conductance studies that the presence of the indoles stabilizes the polypeptide in the bilayer leaflet (M. D. Becker and O. S. Anderson, personal communication). Furthermore, the indole dipole moments have been implicated in cation conductance by functional studies, and the dipole moment orientations have been characterized through structural studies (Hu et al., 1993). To maintain the dipole moment orientations, the side chains need to be fixed in position relative to the channel axis. Consequently, the packing of the leucine and valine side chains about the indole may be functionally significant as a mechanism for fixing the conformation of the indole rings. The two valines in closest proximity to the indoles are fixed in unique rotameric states.

MATERIALS AND METHODS

Sample Preparations. The L-Val-d_8 and DL-Val-d_8 amino acids were obtained from Cambridge Isotope Lab. The D and L mixtures were partially resolved by an enzymatic method (Teng et al., 1991) in order to obtain a higher content of the D form (~70%). The deuterated valine was blocked with a 9-fluorenylmethoxycarbonyl (Fmoc) protecting group on the amino group. The L- or D-Fmoc-Val-d_8 was incorporated into the 1, 6, 7, and 8 residues of gramicidin by using an ABI 430A solid phase peptide synthesizer (Fields et al., 1988, 1989). The products of L-Val_1-d_8- and L-Val_7-d_8-labeled gramicidin gave about 700 mg and were 98% pure upon cleavage from the resin. They were used without further purification. D-Val_6-d_8- and D-Val_8-d_8-labeled gramicidin had a purity of about 70%, which was purified using a preparative C-18 reverse phase HPLC column with two 350 mg sample injections [this procedure represents a scaled-up version of previous purification protocols (Fields et al., 1989)].

Samples were prepared by dissolving 50 mg of gramicidin and 145 mg of DMPC (1:8 molar ratio) in 95% methanol/deuterium-depleted water (DDW). This solution was lyophilized overnight, and approximately 40% by weight DDW was added to the powder sample. To ensure the complete conversion of gramicidin to the channel conformation, the samples were stored for 2 weeks at 45 °C with the samples sealed. The preparations of oriented and unoriented samples were the same, except that for the oriented samples the organic solution was spread onto 20 glass coverslips (5 × 20 mm) having 2 mm wide spacers at each end. These glass coverslips were air-dried overnight and then dried under vacuum to remove residual solvent. The samples were prepared to 50% by weight DDW after the glass plates were stacked in a section of square glass tubing. Incubation at 45 °C for 2 weeks was carried out after the samples were sealed.

^2H Solid State NMR Experiments. All ^2H NMR spectra were obtained on a 9.4 T wide-bore magnet with a Chemagnetics data acquisition system and a homebuilt radio-frequency section. A homebuilt variable temperature probe was tuned to 61.5 MHz. The temperature measurement was taken by locating thermocouples close to the sample coil area for both the inlet and outlet of nitrogen gas. The standard eight-phase cycling quadrupole echo pulse sequence (Davis et al., 1976) was employed. A 30 μs echo delay was used to avoid probe ringing. The experimental conditions include a 2.8 μs $\pi/2$ pulse width, a 1 μs dwell time, and a 0.7 s repetition delay. An additional 1.4 μs (half of the pulse width) postecho delay was used to shift the starting point of the acquisition to the top of the echo. All spectra were processed using FELIX software (Hare Research Inc.).

Computations. All of the programs were written in FORTRAN. The conformation search for Val_1 gramicidin and Val_7 gramicidin was done by the Levenberg–Marquardt least-squares method, in which the minimum deviation was achieved with downhill steps of variable step length. To ensure that the global minima were reached, the search was always repeated with a number of different starting points. These starting points were distributed over the range of possible solutions. For Val_6 and Val_8 gramicidins, the solutions were searched by mapping the full conformational space. Only the solution pairs β_2 and γ_2 were obtained by the least-squares algorithm. The computations were performed on an SGI Indigo II and an IBM RS6000/580.

RESULTS

The structural solution for the side chains requires a separation of dynamic and structural effects for the quadrupolar observations. The influence of global motion can be eliminated from the spectra by lowering the temperature of the gramicidin/lipid preparations to below the gel to liquid-crystalline phase transition temperature of 28 °C (Nicholson et al., 1987). At 5 °C the global correlation time is reduced to the second time scale (Lee et al., 1993) and no longer averages the quadrupolar interactions observed here. Figure 1 shows the ^2H NMR powder pattern spectra of the fully deuterated Val_1, Val_6, Val_7, and Val_8 gramicidins in hydrated DMPC lipid bilayers, recorded at 5 °C. Because spectral sensitivity for $C_\alpha D$ and $C_\beta D$ for all valine sites was low, the methyl intensity, which is averaged by methyl group rotation, dominates in the region between −40 and +40 kHz. These

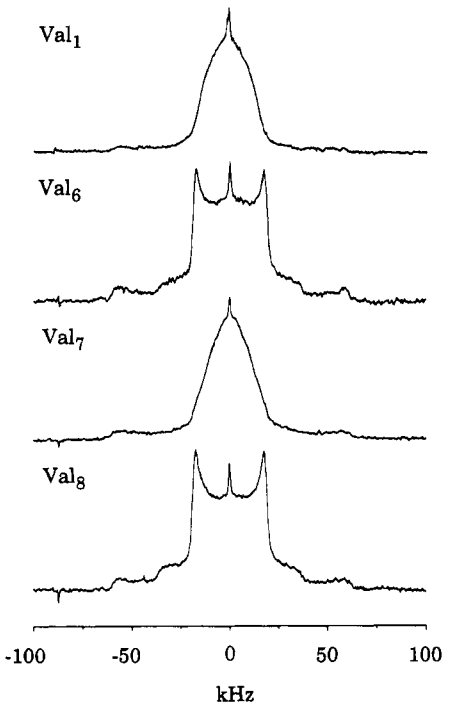

FIGURE 1: ^{2}H NMR powder pattern spectra of d_8-labeled (α, β, γ_1^3, γ_2^3) $Val_{1,6,7,8}$ gramicidins in hydrated DMPC lipid bilayers recorded at 5 °C. The spectra were obtained with approximately 60 000 acquisitions using a 30 μs τ value in the quadrupole echo pulse sequence and a 700 ms recycle delay. The C_α and C_β resonances are reduced in intensity, in part due to a long 90° pulse (resulting from a relatively large coil) and in part due to unfavorable relaxation properties (Hing et al., 1990).

spectra are only subject to local motions. The rotation of the $C_{\gamma_1}D_3$ and $C_{\gamma_2}D_3$ methyls average the ^{2}H Pake powder pattern line widths by a factor of 3 in all cases. The fast librational motions further average the spectral line shape. If fast rotation or jumps occurred about the $C_\alpha-C_\beta$ bond axis, the ^{2}H NMR powder pattern would be averaged by an additional factor of 3, assuming perfect tetrahedral geometry. The Pake patterns for Val_6 and Val_8 present no evidence for large amplitude motions about χ_1; however, Val_1 and Val_7 spectra show intermediate time frame ^{2}H NMR powder line shapes. The χ_1 motion for Val_1 was determined by spectral simulation to be a three-state jump in the intermediate time frame with unequal occupancy of the states (Lee & Cross, 1994). The methyl groups of Val_7 display a similar powder pattern spectrum.

Figure 2 shows the spectral simulation for the two sites undergoing large amplitude motions. Best-fit simulations are shown, as well as the superposition of two sets of simulations, illustrating the sensitivity of the line shapes to the conformational substate population distribution. The populations of the three states are represented by two independent variables that the line shape can uniquely define since the intermediate time frame averaging results in changes in both shape and width. The simulations shown in Figure 2B illustrate that the line shape is very sensitive to the substate with the minimum population and that a population of 10% ± 5% represents the best fit and error bar for the population of this state in Val_1. Figure 2D shows that the states with higher populations have somewhat larger error bars, but they are also sensitive to line shape features. The range for the dominant conformational substate in Val_7 is 64% ± 10%. It should also be noted that the population distributions are significantly different for Val_7 and Val_1.

Oriented samples were prepared to determine the valine side chain conformations and potentially to refine the population distribution. The gramicidin channel axis of the

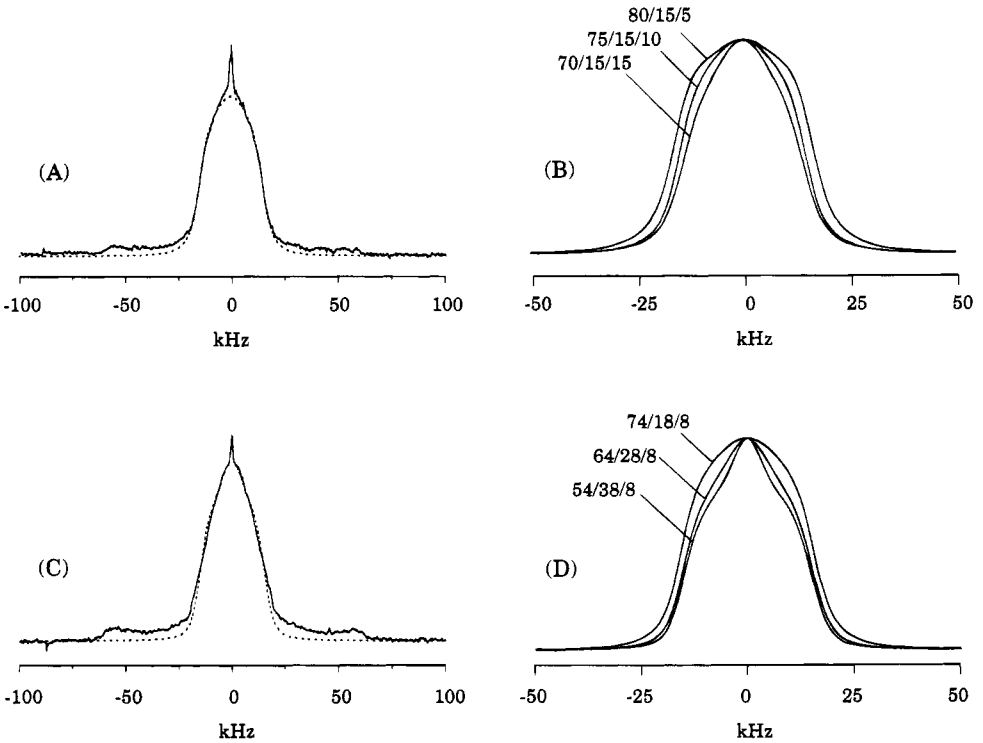

FIGURE 2: Simulation of the powder pattern data from Figure 1 for Val_1 (A and B) and Val_7 (C and D). Best-fit simulations are shown as dashed lines in parts A and C and in the middle of the population range illustrated in parts B and D. (B) This range of population distribution for Val_1 illustrates the error range and high sensitivity of the line shape to the least populated state. (D) This range of population distribution for Val_7 illustrates the error range for the least sensitive states.

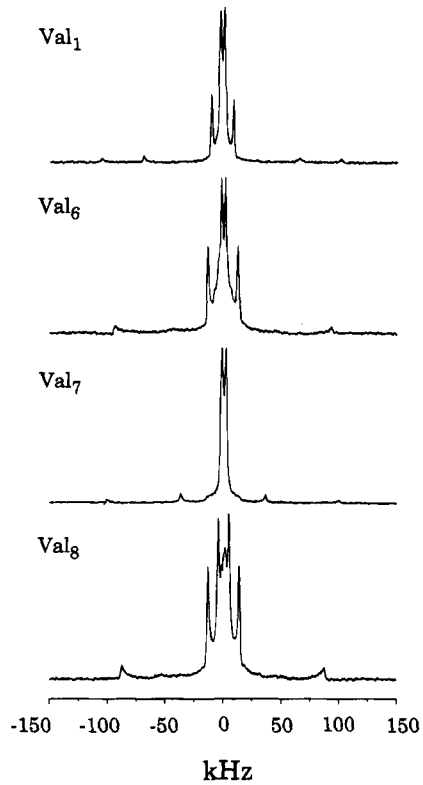

FIGURE 3: ^{2}H NMR spectra of d_8-labeled (α, β, $\gamma_1{}^3$, $\gamma_2{}^3$) $Val_{1,6,7,8}$ gramicidins in oriented DMPC lipid bilayers recorded at 36 °C. The spectra were obtained with approximately 40 000 acquisitions using a quadrupole echo pulse sequence. The quadrupole splittings are listed in Table 1. The C_α and C_β resonances are reduced in intensity due to a long 90° pulse and unfavorable relaxation properties (Hing et al., 1990).

Table 1: Observed ^{2}H Quadrupole Splittings from Uniformly Aligned Samples of Valine-d_8-Labeled Gramicidin in Hydrated Lipid Bilayers[a]

	Val_1	Val_1 at 22 °C	Val_6	Val_7	Val_8
$C_\alpha D$	+205	+205	+187	+200	+174
$C_\beta D$	+133	+133	+187	+71	+174
$C_{\gamma_1}D_3$	+3.8	+6.6	+3.3	+3.8	+8.1
$C_{\gamma_2}D_3$	+19.1	+19.4	−26.1	+3.8	−27.3

[a] Data were recorded at 36 °C except where noted.

oriented samples has been aligned parallel to the magnetic field of the NMR spectrometer. In this way, the orientation of the electric field gradient (EFG) tensor elements with respect to the field will be the same as their orientation with respect to the channel axis. Figure 3 shows the quadrupole splittings for oriented samples of the d_8-labeled Val_1, Val_6, Val_7, and Val_8 gramicidin A's. Splitting values were obtained for $C_{\gamma_1}D_3$, $C_{\gamma_2}D_3$, $C_\beta D$, and $C_\alpha D$ in each sample, and the data are summarized in Table 1. These assignments were determined from calculations to be described later. The $C_\beta D$ and $C_\alpha D$ splittings for Val_6 and Val_8 were not resolved due to spectral overlap. In comparison with the powder pattern data recorded below the lipid phase transition temperature, it is clear that the Val_6 and Val_8 residues in the oriented samples at 36 °C represent spectra in fast exchange. Consequently, the residence times in the conformational substates have decreased from the microsecond to the nanosecond time scale upon raising the temperature.

Characterization of the EFG tensor and assessment of librational averaging is critically important for this structural analysis. The QCC of a static CD site in L-alanine-d_3 crystalline powder was determined to be 171 ± 5 kHz at −135 °C (Keniry et al., 1984) and estimated to be 165 kHz (Jelinski et al., 1980) and 167 kHz (Beshah et al., 1987) by others. For deuterium NMR studies of gramicidin, a QCC of 168 kHz was used for $C_\alpha D$ (Prosser et al., 1991; Hing et al., 1990a) and for the Val_1 side chain (Killian et al., 1992). The asymmetry parameter η is typically very small for aliphatic C−D bonds (approximately 0.05) and has been assumed to be zero here. Slight asymmetry would have little impact on the calculations described. The static QCC value will be reduced due to librational motions. These amplitudes are anticipated to be dependent on the site within the side chain. The farther away from the backbone, the greater the librational amplitude. From Figure 1, unique spectral features are clearly seen in three of the four spectra at ±61 kHz. These features have been assigned to the C_α deuterons, because these sites are assumed to be more rigid than the C_β deuterons. The 61 kHz features correspond to a quadrupole coupling constant of 163 kHz, which is consistent with the C_α data from the alanine (Lee et al., 1993) and leucine (Lee, 1994) sites in gramicidin. This value has been used for all four valines, representing an assumption for only the Val_1 site. The QCC for the C_β deuterons cannot be readily obtained from the valine spectra since these signals overlap with the C_α deuterons, and the QCC is expected to have a slightly reduced magnitude for the $C_\beta D$ sites. A slightly reduced splitting for $C_\beta D$ would not be well-defined by the data in Figure 1. Consequently, the librational averaging of the C_β methyl deuterons of alanine-d_4 labeled gramicidin (Lee et al., 1993) was used after accounting for the factor of 3 reduction in interaction magnitude caused by methyl rotation (51 × 3 = 153 kHz). This value is also consistent with the QCC values for the β-deuterons on the leucine side chains (Lee, 1994). The librational averaged QCC for the valine methyl groups was obtained from the powder spectra of Val_6- and Val_8-labeled gramicidin at 5 °C, as shown in Figure 1 (48.3 × 3 = 145 kHz).

A model for the local dynamics therefore is described for each of the valine sites in the gramicidin channel. Once the motional averaging of the tensors is described, the structural constraints can be derived from the spectra of oriented samples. The error bar for the orientational constraints increases with increasing motional averaging; consequently, the structure of these side chains will be determined by starting at the backbone structure and working outward. Because the backbone structure has been determined from numerous constraints in the peptide planes, the orientations of the C_α−H and C_α−C_β bonds are known from independent results for each of the valine residues. This information is used in combination with the $C_\alpha D$ splitting. The unique determination of these bond orientations is achieved with additional quadrupole splittings from the side chain. Once a solution for these angles is found, χ_1 is determined from further analysis of $C_\beta D$, $C_{\gamma_1}D_3$, and $C_{\gamma_2}D_3$ splittings.

Constraints for β_2 and γ_2 Angles. Figure 5 shows the possible pairs of β_2/γ_2 angles (see Figure 4 for definitions) for Val_1, Val_6, Val_7, and Val_8, calculated from the $C_\alpha D$ splittings. Larger $C_\alpha D$ quadrupole splittings generate more restrictive β_2/γ_2 solution sets and, hence, smaller β_2/γ_2 ellipses. The β_2 symmetry about 70° and 110° and the γ_2 symmetry about 180° and 0° result in β_2/γ_2 pairs that compensate for each other to maintain the quadrupole

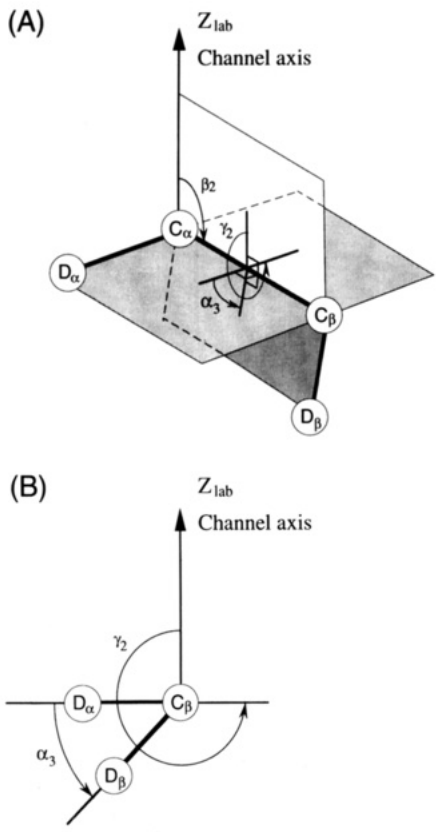

FIGURE 4: (A) β_2 is defined as the angle between the $C_\alpha-C_\beta$ bond axis and the external magnetic field and channel axis. γ_2 is defined as the angle between the $z_{LAB}-C_\alpha-C_\beta$ and $D_\alpha-C_\alpha-C_\beta$ planes. α_3 is defined as the angle between the $D_\alpha-C_\alpha-C_\beta$ and $C_\alpha-C_\beta-D_\beta$ planes. (B) Projection view down the $C_\beta-C_\alpha$ axis. The value of α_3 will be the same as χ_1 for an L form residue and $\chi_1 - 240°$ for a D form residue.

splitting value. The β_2 and γ_2 angles for each of the valines from the channel backbone structure are shown in Table 2. Because the backbone structure has not been refined with motionally averaged tensors, the values of β_2/γ_2 need to be used here as constraints rather than as absolute determinations. An error bar of $\pm 10°$ was considered for each of these values derived from the backbone, and these are shown by the boxes in Figure 5. It is immediately clear that the Val_1 and Val_7 solutions are restricted to the ellipse with γ_2 symmetry centered on 180° and that the Val_6 and Val_8 solutions are restricted to the ellipse with γ_2 symmetry centered on 0°. It is also seen that, with such error bars, for each residue a single β_2 value defines a unique γ_2 solution.

Val_6 and Val_8 Side Chain Conformations. With β_2 and γ_2 highly constrained, the additional orientational constraints of $C_\beta D$, $C_{\gamma_1}D_3$, and $C_{\gamma_2}D_3$ were used to generate a unique solution. Shown in Figure 6 are plots of β_2/γ_2 solutions versus χ_1, the angle that is derived directly from α_3. The contours represent root mean square deviations between the observed methyl splitting values and those calculated from the β_2, γ_2, and χ_1 angles. Since the assignments of the quadrupole splittings have not been achieved, the rms deviations were calculated using all possible assignments and either positive or negative splitting values where appropriate. If the splitting magnitude is greater than $^3/_4$QCC, it must have a positive sign. Only the minimum rms deviations are plotted in Figure 6.

In each of these plots there are four deep minima in the entire span of χ_1 space. These minima are all in the vicinity of the $\chi_1 = 60°$ rotameric state. For Val_6 the $\Delta\nu_{obs}$ for $C_{\gamma_2}D_3$ is -26 kHz and for $C_{\gamma_1}D_3$ it is $+3$ kHz. Two of these minima are inconsistent with the associated $C_\beta D$ splitting. Note that the calculated value of the $C_\beta D$ splitting is dependent on the β_2/γ_2 values for the observed minima, and therefore two $C_\beta D$ curves are drawn, one for a β_2 of 88° and one for a β_2 of 83°. Since the two solutions that yield reasonable predicted values for $C_\beta D$ splittings have a single β_2 value, both β_2 (88°) and γ_2 (16°) are uniquely defined for Val_6. This 25 kHz difference (45 kHz for Val_8) in the calculated values of the $C_\beta D$ splitting shows that the conclusions of this analysis are insensitive to the exact value of the $C_\beta D$ QCC value, since it would take more than a 10% change in QCC to effect such a change in the splitting. This is the one QCC value obtained from non-valine sites in the gramicidin channel and the one site susceptible to a significant (up to 5% error). The two possible χ_1 values are 34° and 55°. Of these, $\chi_1 = 55°$ is the most probable since the other possibility is 26° from the stable rotameric state. The analysis for Val_8 is very similar, leading to the assignment of $C_{\gamma_2}D_3$ to the -27 kHz splitting, while the $\Delta\nu_{obs}$ for $C_{\gamma_1}D_3$ site is assigned to the $+8$ kHz splitting. Again, four contour minima are found in the entire χ_1 conformational range, and only two of these minima are consistent with the $C_\beta D$ splittings. Both solutions have the same β_2 (90°) and γ_2 (17°) angles. Furthermore, the χ_1 solution of 30° is 30° from the rotameric state, and therefore the most probable solution has a χ_1 of 55°, just 5° from the rotameric state.

Val_1 and Val_7 Side Chain Conformations. As described previously, these two side chains have been shown to undergo intermediate time frame motions at 5 °C and fast exchange motion at 36 °C, which is above the gel to liquid-crystalline phase transition temperature. Not only the rate of exchange but also the populations may change between these two temperatures. If the populations do change, it is anticipated that the populations will become somewhat more equal. Therefore, the populations of the conformational substates determined at 5 °C are used as a restricted variable in defining the conformations of these states from the quadrupole splittings. Because the three populations are normalized, there are two restricted variables to be considered for the populations. In fast exchange the quadrupolar splittings will be further averaged by the jump motions. Each jump is assumed to be a 120° rotation about the $C_\alpha-C_\beta$ axis. Expressions for the splitting values in the presence of these motions are developed in the Appendix.

As shown in Figure 5, the values of β_2 and γ_2 are highly constrained for Val_1 and Val_7 by the $C_\alpha D$ splitting and knowledge of the backbone structure. Since a unique solution is defined for each β_2 value, γ_2 is not a variable and β_2 is a restricted variable. α_3, which is equivalent to χ_1, is the final variable. Shown in Figure 7 is a plot of Val_1 populations versus χ_1. At 36 °C, only $\beta_2 = 106°$ generates solutions that satisfy all of the quadrupole splitting constraints. Therefore, the entire solution set for the remaining variables is displayed in this figure. Two factors can be used to further restrict the solution set. First, if the populations that have been accurately defined at 5 °C change upon increasing the temperature, it is assumed that the populations will tend toward equalization. Therefore, a minimum population of 10% ± 5%, defined by the 5 °C data set in Figure 1, can be assumed to represent the minimum population at 36 °C as well. A constraint at 5% substantially

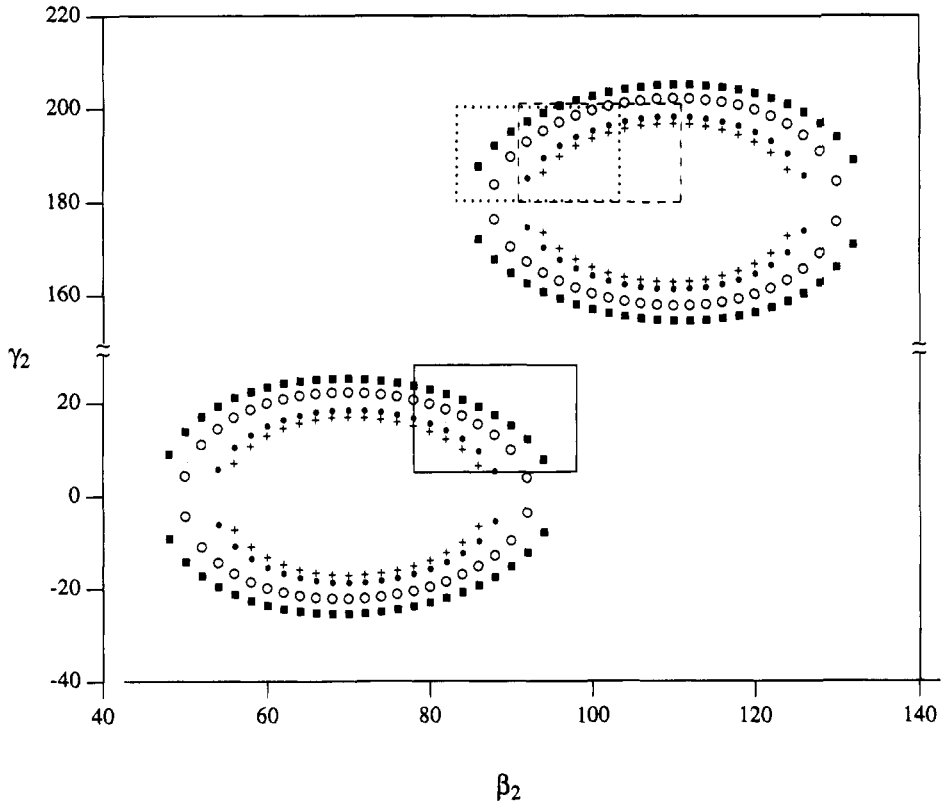

FIGURE 5: Plot of β_2 versus γ_2 for Val_1 (+), Val_6 (○), Val_7 (●), and Val_8 (■). This plot was generated from all of the possible solutions for the $C_\alpha D$ quadrupolar splitting. A larger splitting will lead to a smaller angle between $C_\alpha D$ and z_{LAB} and, therefore, a smaller ellipse centered on either $\gamma_2 = 180°$ or 0°. β_2 and γ_2 values obtained from the backbone structure were used as constraints, with an error bar of ±10° defining the boxes shown.

Table 2: Structural Parameters (Degrees) from Side Chain ^2H and Backbone ^{15}N Analyses

	Val_1			Val_6			Val_7			Val_8		
	β_2	γ_2	χ_1	β_2	γ_2	χ_1	β_2	γ_2	χ_1	β_2	γ_2	χ_1
^{15}N	101	190		88	18		93	189		88	15	
^2H	106	198	177[a]	88	16	55	103	199	215[a]	90	17	55

[a] Only the dominant rotameric state is listed.

reduces the solution set to the boxed regions in Figure 7. Second, those solutions that are more than 20° from the rotameric state are deemed to be unlikely, especially in light of possible solutions in the immediate vicinity of the rotameric state. β-Branched amino acid side chains have their χ_1 torsional space substantially reduced by steric constraints with the polypeptide backbone (McGregor et al., 1987). Furthermore, the conformational states observed from very high-resolution crystallographic studies are primarily restricted (>85%) to this range in the vicinity of the rotameric states (Lee & Cross, 1994). Therefore, the conformational solution for the dominant component is $\chi_1 = 177° \pm 7°$, and the populations are 78% ± 3%, 13% ± 7%, and 9% ± 4%. These populations are within experimental error of those determined at 5 °C by the independent approach described in Figure 1. The data in Table 1 for Val_1 at 22 °C also fit with a single value of β_2 (103°) that is just 3° different from the value required to fit the data at 36 °C. This suggests that a small structural change may be occurring upon cooling the sample down into the middle of the sample phase transition temperature range, which is broad due to the high molar ratio of gramicidin to lipid (1:8). Other differences displayed in Figure 7 for these two temperatures represent very minor differences either in χ_1 or in the populations of the three states.

Figure 8 displays the χ_1 and population solution set for Val_7. Again, a single β_2 solution is found (103°). Due to the smaller $C_\beta D$ splitting for this residue compared to Val_1, the solution set for the remaining variables is much greater. However, from this entire set of solutions two regions are viable. Solutions that are within 20° of the χ_1 rotameric state of 180° represent one region, with populations of 48% ± 3%:35% ± 10%:17% ± 10%. Despite this 40° range in χ_1, the populations are quite well-defined. A second solution range is in the vicinity of $\chi_1 = 215°$, where the populations are within experimental error of those determined at 5 °C: 61%, 28%, and 11%. There is a similar solution at $\chi_1 = 227°$, which is almost an eclipsed conformational state; even the $\chi_1 = 215°$ solution is 35° from the rotameric state. However, since there is no evidence that the populations changed between 5 and 36 °C for Val_1, the 215° solution should be considered as a viable, if not probable, solution.

DISCUSSION

Recently, Ruterjans and co-workers used solution NMR-derived *J* coupling constraints to characterize the structure and dynamics of valines in ribonuclease T_1 (Karimi-Nejad et al., 1994). There are many challenges to be overcome in using *J* coupling constraints quantitatively. These authors have made considerable progress in this regard. While models for molecular motion were assumed and tested in this ribonuclease T_1 study, the effort presented here by solid state NMR on a polypeptide in a fully hydrated lipid bilayer

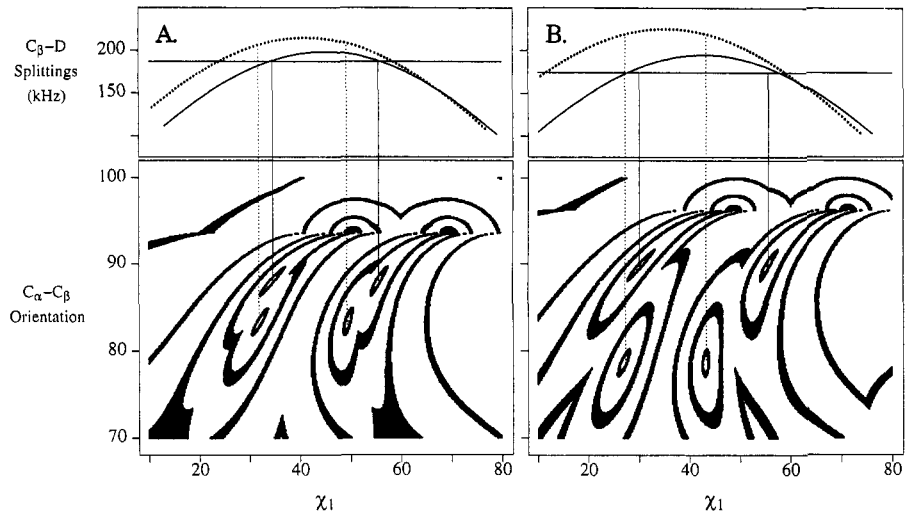

FIGURE 6: Determination of the Val_6 (A) and Val_8 (B) conformational parameters. β_2 (C_α–C_β orientation) versus α_3 ($\chi_1 - 240°$) for each residue. The contour plots represent the rms deviations between calculated and observed methyl quadrupole splittings. The rms deviation displayed represents the minimal deviation calculated using all possible assignments and quadrupole splitting signs. The observed $C_\beta D$ quadrupole splitting is shown as a horizontal line in the top panel, and the curves represent calculated $C_\beta D$ splittings for two different values of β_2. The rotameric state within the χ_1 space displayed is 60°.

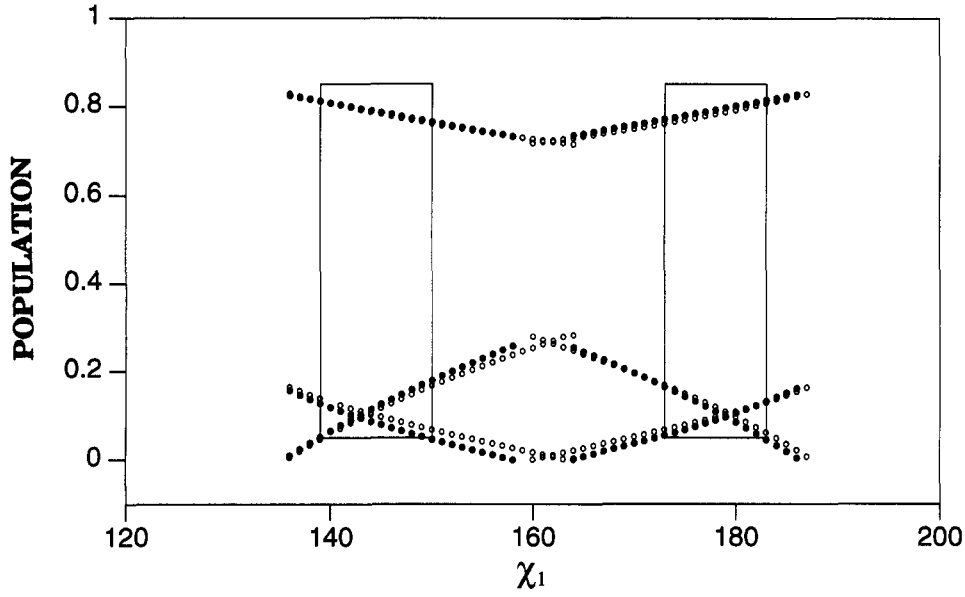

FIGURE 7: Structural and dynamic parameter set for Val_1. The only solutions for this residue at 36 °C (●) had unique solutions for β_2 (106°) and γ_2 (198°). The minimum population for a conformational state was established as 5% on the basis of Figure 2. This restricts the solution set to the boxed regions. Data for 22 °C (○) were also analyzed, and the only solutions have β_2 (103°) and γ_2 (199°) uniquely defined.

determined the motional model in detail and the structure of the valine residues from independent data sets. In this way, the librational amplitude for each torsional segment of the side chain is determined, large amplitude motions about the torsion angles are determined, and the torsion angles are defined in light of the experimentally described motions.

Table 2 summarizes the conformational data determined in this study for the four valine residues per monomer of the gramicidin channel. The data are compared to the results from the published backbone structure determination (Ketchem et al., 1993). For Val_6 and Val_8, the values of β_2 and γ_2 are virtually identical. For the two residues that show large amplitude motions, Val_1 and Val_7, significant differences occur. For Val_1, β_2 and γ_2 values differ by 4° and 6°, respectively, and for Val_7, the values both differ by 10°. A partial explanation for this is that the backbone structure was determined without explicitly taking librational motions into consideration; such an effort is underway and may bring these two determinations closer together.

The dynamics and structural characterization of Val_1 that has previously been published (Lee & Cross, 1994) is virtually identical to that achieved here using a different analysis approach and different assumptions. Small differences result from the more accurate determination of the librationally averaged QCC values. The powder pattern data for $C_\alpha D$ in Figure 1 show significantly better discontinuities from Val_6, Val_7, and Val_8 than from Val_1. The temperature dependence of the Val_1 data (Killian & Koeppe, 1992; Lee & Cross, 1994) has now been rationalized by solving for the entire parameter set at the two distinctive temperatures (36 and 22 °C). It is apparent that a small structural change occurs that can completely account for the near doubling in the $C_{\gamma_1}D_3$ splitting while $C_{\gamma_2}D_3$ remains constant. Such a structural change could be associated with the expansion of

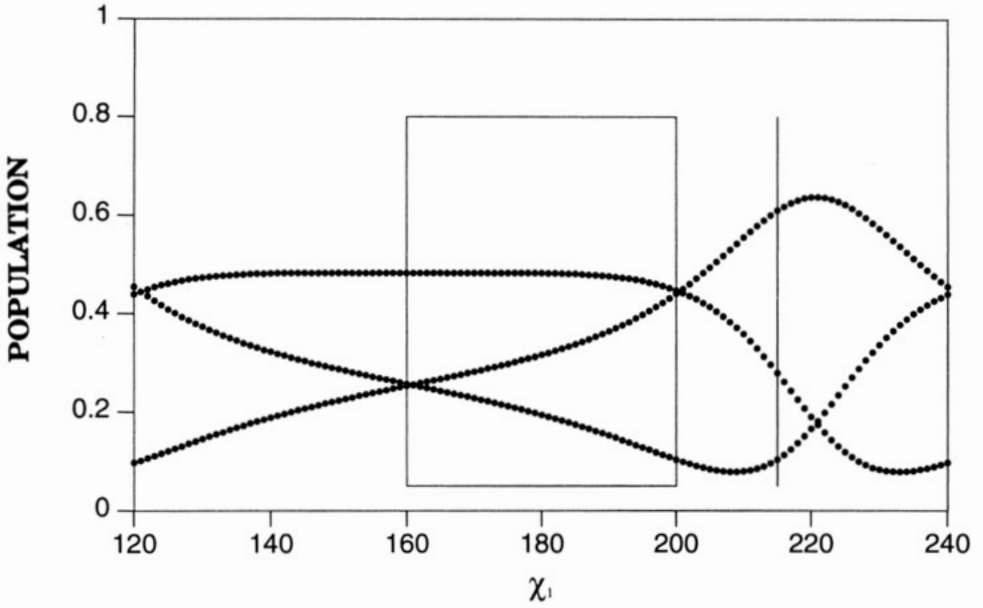

FIGURE 8: Structural and dynamic parameter set for Val_7. The only solutions for this residue at 36 °C (●) have β_2 (103°) and γ_2 (199°) uniquely defined. Two viable solution sets for χ_1 and the conformational states can be described. One is in the vicinity of the 180° rotameric state and the other ($\chi_1 = 215°$) has the population distribution observed at 5 °C.

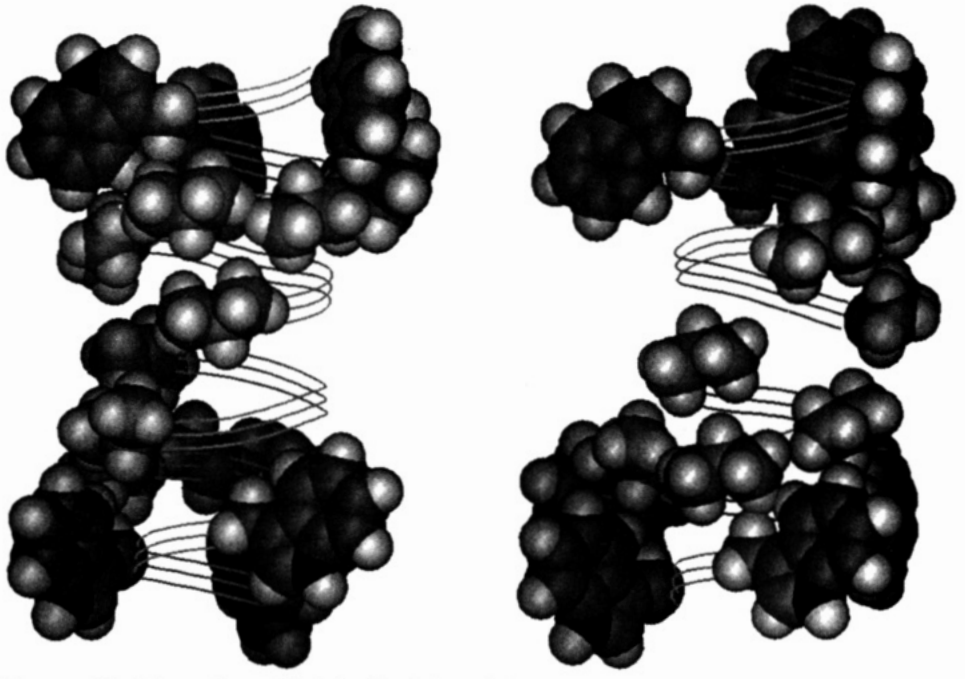

FIGURE 9: Space-filling model of the valine and indole side chains of the gramicidin channel structure from two different side views. The Val_1 and Val_7 side chains are shown in their dominant conformations, and for Val_7 and χ_1 angle used for these illustrations was 180°, but 215° does not cause additional steric hindrance with the other side chains. It is shown here that Val_6 and Val_8 pack closely against the indole rings.

the bilayer hydrophobic dimension upon entering the gel state (the transition temperature is approximately 28 °C and is very broad). It is interesting to note that the structural change that is observed is a change in the backbone structure rather than the side chain structure. Once again, the high sensitivity of this spectroscopy for providing structural and dynamic constraints should be noted.

The dynamics of the valine side chains appears to correlate very well with steric hindrance from the adjacent side chains. As shown in Figure 9, Val_6 is within van der Waals contact with Trp_{13}, and Val_8 contacts both Trp_9 and Trp_{15}. Until the indole conformations have been refined, these results should be viewed as preliminary conclusions, but it appears that the packing of Val_6 and Val_8 next to the indoles may be the explanation for why these two sites are restricted to a single rotameric state. This interaction with the indole rings may have significant functional implications. The orientation of the indole dipole moments has a direct and very significant impact on the conductance rate of the channel. It appears that these valine residues help to maintain the dipole orientation by being closely packed against the indoles. The reasoning presented earlier for the static nature of Val_6 and Val_8 while Val_1 and Val_7 are dynamic further supports the assignment of our most probable indole conformational states.

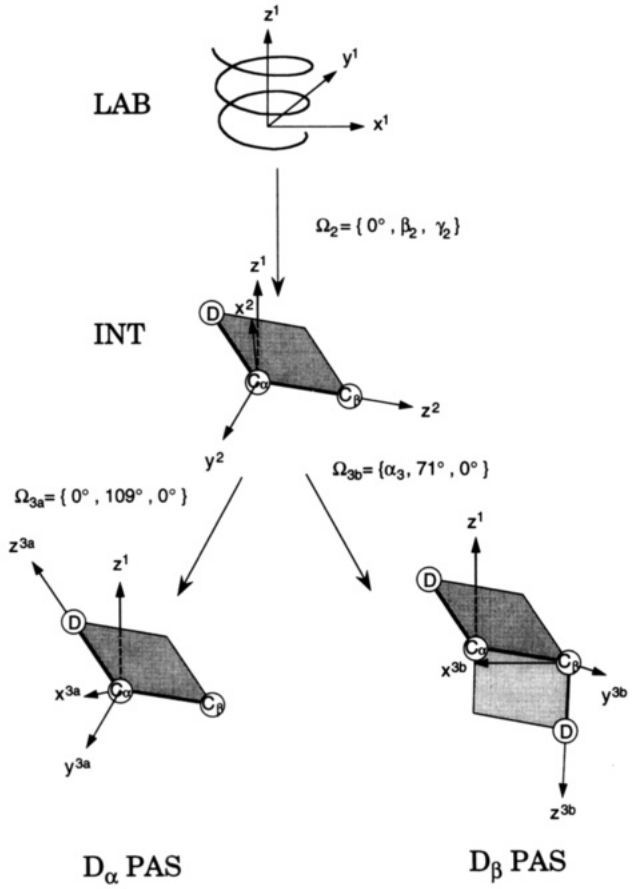

FIGURE 10: Tensor transformations from the laboratory frame (LAB) to the principal axis system (PAS). For the LAB frame, z^1 is defined parallel to the channel axis and y^1 and x^1 complete the orthogonal set. The intermediate frame (INT) is defined with z^2 along the $C_\alpha-C_\beta$ bond, x^2 in the plane formed by $D_\alpha-C_\alpha-C_\beta$, and y^2 completes the set. z^2 is rotated about y^2 to achieve z^{3a} along $C_\alpha D$. The $C_\beta D$ PAS frame is defined with z^{3b} along the $C_\beta-D$ bond, x^{3b} in the plane formed by $C_\alpha-C_\beta-D$, and y^{3b} completes the set. These tensor transformations were performed using the Ω_1, Ω_2, and Ω_3 Euler angles where β_2, γ_2, and α_3 are the variables.

It is concluded here that the dynamics of these side chains are not correlated with the fluidity of the membrane environment as a function of depth into the bilayer. This establishes a virtual dynamic phase boundary between the lipid and the peptide that is further supported by unpublished results that show Leu_4 to be fixed in a single rotameric state (K.-C.L., S.H. and T.A.C.). In other words, there is little interaction between the lipid and the peptide in the hydrophobic environment. This is further supported by the modest changes in Val_1 dynamics as a function of temperature. There is, however, interaction between the side chains; some of the other pairs of rotameric states (other than the trans states) for Val_7 and Val_1 show atomic overlap with each other. This raises the exciting possibility that the dynamics for these two side chains are correlated with each other. The correlation is not absolute because the populations for the three rotameric states of each residue differ significantly. However, weak correlations are implicated, in that certain pairs of conformational states appear to represent lower energy (less steric hindrance) states.

ACKNOWLEDGMENT

We are deeply indebted to the staff of the FSU NMR Facility, J. Vaughn, R. Rosanske, and T. Gedris, for their skillful maintenance of the facility and spectrometers and to the staff of the Bioanalytical Synthesis and Services Facility, H. Henricks and U. Goli, for their expertise and maintenance of the ABI 430A peptide synthesizer and HPLC equipment.

APPENDIX

Quadrupolar Splittings in the Absence of Motional Averaging. The equilibrium Hamiltonian for an ensemble of deuterons in a magnetic field is (Cohen & Reif, 1957)

$$H_0 = H_{0z} + \sum_{M=-2}^{2} (-1)^M A_{-M}^{(2)} T_M^{(2)\mathrm{LAB}} \qquad (1)$$

where H_{0z} is the Zeeman interaction energy, $A_M^{(2)}$ are the spin operators, and $T_M^{(2)\mathrm{LAB}}$ are the spherical, irreducible components of the quadrupole coupling tensor in the lab-fixed frame. The components of the quadrupole coupling tensors are only known as constants in the principal axis system, where they can be written as

$$T_0^{(2)\mathrm{PAS}} = \frac{\sqrt{6}}{4}\mathrm{QCC}, \quad T_{\pm1}^{(2)\mathrm{PAS}} = 0, \quad T_{\pm2}^{(2)\mathrm{PAS}} = {}^1/_4\eta\mathrm{QCC}$$

where QCC is the effective quadrupole coupling constant, $\langle e^2qQ/\hbar\rangle$, and η is the asymmetry parameter. With the high-field approximation, only the secular term is needed. The quadrupole splittings, $\Delta\nu_Q$, can be written as (Vega & Pine, 1977)

$$\Delta\nu_Q = \sqrt{6}T_0^{(2)\mathrm{LAB}} \qquad (2)$$

The quadrupole tensor component, $T_0^{(2)\mathrm{LAB}}$, can be evaluated in terms of the quadrupole coupling constant and the asymmetry parameter by doing proper transformations from the laboratory frame to the principal axis system.

To simplify the orientational complexity, and to show the relationship between axes, an intermediate axis system is defined, as shown in Figure 10, with the z^2 axis collinear with the $C_\alpha-C_\beta$ bond, the y^2 axis defined by the cross product of z^2 and the vector $C_\alpha-D$, and x^2 completes the orthogonal set. Then, the transformation from the laboratory frame to the PAS of $C_\alpha D$ is

$$\mathrm{LAB} \xrightarrow{\Omega_1} \text{channel} \xrightarrow{\Omega_2} \text{intermediate} \xrightarrow{\Omega_{3a}} \mathrm{PAS}\ (C_\alpha D)$$

In the case of oriented samples, the channel z^1 coincides with the LAB z axis and it is uniaxial. No transformation is needed between these two frames. The Euler transformation angles are

$$\Omega_1 = \{0,0,0\}$$

$$\Omega_2 = \{0,\beta_2,\gamma_2\}$$

$$\Omega_{3a} = \{0,109.5°,0\}$$

The transformation from the LAB to the PAS of $C_\beta D$ is

$$\mathrm{LAB} \xrightarrow{\Omega_1} \text{channel} \xrightarrow{\Omega_2} \text{intermediate} \xrightarrow{\Omega_{3b}} \mathrm{PAS}\ (C_\beta D)$$

The Euler angles are

$$\Omega_1 = \{0,0,0\}$$

$$\Omega_2 = \{0,\beta_2,\gamma_2\}$$

$$\Omega_{3b} = \{\alpha_3,70.5°,0\}$$

As illustrated in Figure 4, the angle α_3, which is the angle between the $D_\alpha-C_\alpha-C_\beta$ and $C_\alpha-C_\beta-D_\beta$ planes, is related to the torsion angle, χ_1, by ±120°. The tilt angle, β_2, represents the tilt angle of the $C_\alpha-C_\beta$ bond with respect to the external magnetic field (z_{LAB}) or the channel axis, and γ_2 represents the tilt angle between the $D_\alpha-C_\alpha-C_\beta$ plane and the plane formed by the $C_\alpha-C_\beta$ bond and the $C_\alpha-z_{LAB}$ axis. The Euler angles and transformations are defined following the Rose convention for irreducible spherical tensors (Rose, 1957). In the absence of motional averaging, the quadrupole tensors in the LAB frame for D_α and D_β are

$$T_0^{(2)LAB} = T_0^{(2)helix} = \sum_{m=-2}^{2}\sum_{n=-2}^{2} D_{0m}^{(2)*}(\Omega_2)D_{mn}^{(2)*}(\Omega_3)T_n^{(2)PAS} \quad (3)$$

and the quadrupole splittings are

$$\Delta\nu_Q = \sqrt{6}\sum_{m=-2}^{2}\sum_{n=-2}^{2} D_{0m}^{(2)*}(\Omega_2)D_{mn}^{(2)*}(\Omega_3)T_n^{(2)PAS} \quad (4a)$$

For deuterons attached to carbon, the asymmetry parameters are typically less than 0.05. Therefore, it is a reasonable approximation to neglect η, and the explicit expression for the splittings is reduced to

$$\Delta\nu_Q = {}^3/_8QCC\{(3\cos^2\beta_2 - 1)(3\cos^2\beta_3 - 1) - 3\sin 2\beta_3 \cos 2\beta_2 \cos(\alpha_3 + \gamma_2) + 3\sin^2\beta_3 \sin^2\beta_2 \cos 2(\alpha_3 + \gamma_2)\} \quad (4b)$$

For the valine side chains of gramicidin, the only unknown angles are β_2, γ_2, and α_3. Therefore, if the quadrupole splittings of more than three different deuterons are experimentally available, these conformation angles can be obtained by solving a group of equations derived from eq 4. Since the quadrupole splittings can be measured very reliably, very accurate conformation angles can be obtained in this way.

Quadrupolar Splittings in the Presence of Motional Averaging. In the presence of motion about the $C_\alpha-C_\beta$ bond, the quadrupole tensors of the deuterons on the β-carbon are motionally averaged. The averaging can be described by the third transformation, which is from the $C_\alpha-C_\beta$ intermediate axis to the PAS. Instead of eq 4, the quadrupole splittings can be written as

$$\Delta\nu_Q = \sqrt{6}\sum_{m=-2}^{2}\sum_{n=-2}^{2} D_{0m}^{(2)*}(\Omega_2)\langle D_{mn}^{(2)*}(\Omega_3)\rangle T_n^{(2)PAS} \quad (5a)$$

and if $\eta = 0$, the equation is reduced to

$$\Delta\nu_Q = {}^3/_8QCC\{(3\cos^2\beta_2 - 1)(3\cos^2\beta_3 - 1) - 3\sin 2\beta_3 \cos 2\beta_2\langle\cos(\alpha_3 + \gamma_2)\rangle + 3\sin^2\beta_3 \sin^2\beta_2\langle\cos 2(\alpha_3 + \gamma_2)\rangle\} \quad (5b)$$

where the brackets denote motional averaging. For a three-state jump about the $C_\alpha-C_\beta$ bond, the terms being averaged can be written as

$$\langle\cos(\alpha_3 + \gamma_2)\rangle = \sum_{i=1}^{3} P_i \int \exp(-x^2/\sigma^2)[\cos(\alpha_3^0 + \gamma_2 + (i-1)120°)]\,dx \quad (6a)$$

$$\langle\cos 2(\alpha_3 + \gamma_2)\rangle = \sum_{i=1}^{3} P_i \int \exp(-x^2/\sigma^2)[\cos 2(\alpha_3^0 + \gamma_2 + x + (i-1)120°)]\,dx \quad (6b)$$

where α_3^0 is the first Euler angle for the transformation from the $C_\alpha-C_\beta$ intermediate axis to the first site, i is the index for the state, and σ is the width of the Gaussian distribution at each state. For D_β, the quadrupole splittings can be expressed in terms of the state populations, P_1, P_2, and P_3, and the transformation angles, γ_2 and β_2. The presence of motion introduces additional parameters, and more experimental information is needed to determine the conformation angles. However, with additional knowledge, e.g., powder pattern data or the temperature dependence of the splittings, the solution set can be restricted to a defined range.

REFERENCES

Bechinger, B., Zasloff, M., & Opella, S. J. (1993) *Protein Sci. 2*, 2077−2084.

Beshah, K., Olejniczak, E. T., & Griffin, R. G. (1987) *J. Chem. Phys. 86*, 4730−4736.

Bystrov, V. F., Arseniev, A. S., Barsukov, I. L., & Lomize, A. L. (1987) *Bull. Magn. Reson. 8*, 84−94.

Chiu, S.-W., Jakobsson, E., Subramaniam, S., & McCammon, J. A. (1991) *Biophys. J. 60*, 273−285.

Cohen, M. H., & Reif, F. (1957) *Solid State Physics 5*, Academic Press, New York.

Cross, T. A. (1994) *Annu. Rep. NMR Spectrosc. 29*, 123−167.

Cross, T. A., & Opella, S. J. (1994) *Curr. Opin. Struct. Biol. 4*, 574−581.

Cross, T. A., Ketchem, R. R., Hu, W., Lee, K.-C., Lazo, N. D., & North, C. L. (1992) *Bull. Magn. Reson. 14*, 96−101.

Davis, J. H., Jeffrey, K. R., Bloom, M., Valic, M. I., & Higgs, T. P. (1976) *Chem. Phys. Lett. 42*, 390−394.

Fields, G. B., Fields, C. G., Petefish, J., Van Wart, H. E., & Cross, T. A. (1988) *Proc. Natl. Acad. Sci. U.S.A. 85*, 1384−1388.

Fields, C. G., Fields, G. B., Noble, R. L., & Cross, T. A. (1989) *Int. J. Pept. Protein Res. 23*, 298−303.

Hing, A., Adam, S., Silbert, D., & Norberg, R. (1990) *Biochemistry 29*, 4144−4156.

Hu, W., Lee, K.-C., & Cross, T. A. (1993) *Biochemistry 32*, 7035−7047.

Huo, S., Lee, K.-C., Lazo, N. D., Hu, W., North, C. L., & Cross, T. A. (1994) *Biophys. J. 66*, A220.

Jelinski, L. W., Sullivan, C. E., & Torchia, D. A. (1980) *Nature 284*, 531−534.

Karimi-Nejad, Y., Schmidt, J. M., Ruterjans, H., Schwalbe, H., & Griesinger, C. (1994) *Biochemistry 33*, 5481−5492.

Keniry, M. A., Kintanar, A., Smith, R. L., Gutowsky, H. S., & Oldfield, E. (1984) *Biochemistry 23*, 288−298.

Ketchem, R. R., Hu, W., & Cross, T. A. (1993) *Science 261*, 1457−1460.

Killian, J. A., Taylor, M. J., & Koeppe, R. E., II (1992) *Biochemistry 31*, 11283−11290.

Koeppe, R. E., II, Killian, J. A., & Greathouse, D. V. (1994) *Biophys. J. 66*, 14−24.

Lazo, N. D., Hu, W., Lee, K.-C., & Cross, T. A. (1993) *Biochem. Biophys. Res. Commun. 197*, 904−909.

Lee, K.-C. (1994) Ph.D. Dissertation, Florida State University, Tallahassee, FL.

Lee, K.-C., & Cross, T. A. (1994) *Biophys. J. 66*, 1380−1387.
Lee, K.-C., Hu, W., & Cross, T. A. (1993) *Biophys. J. 65*, 1162−1167.
LoGrasso, P. V., Nicholson, L. K., & Cross, T. A. (1989) *J. Am. Chem. Soc. 111*, 1910−1912.
Lomize, A. L., Orechov, V. Yu., & Arseniev, A. S. (1992) *Bioorg. Khim. 18*, 182−200.
McGregor, M. J., Islam, S. A., & Sternberg, M. J. E. (1987) *J. Mol. Biol. 198*, 295−310.
Nicholson, L. K., Moll, F., Mixon, T. E., LoGrasso, P. V., Lay, J. C., & Cross, T. A. (1987) *Biochemistry 26*, 6621−6626.
Nicholson, L. K., Teng, Q., & Cross, T. A. (1991) *J. Mol. Biol. 218*, 621−637.
Nicholson, L. K., Asakura, T., Demura, M., & Cross, T. A. (1993) *Biopolymers 33*, 847−861.
North, C. L., Cross, T. A. (1993) *J. Magn. Reson. 101B*, 35−43.
Prosser, R. S., & Davis, J. H. (1994) *Biophys. J. 66*, 1429−1440.
Prosser, R. S., Davis, J. H., Dahlquist, F. W., & Lindorfer, M. A. (1991) *Biochemistry 30*, 4687−4696.
Prosser, R. S., Daleman, S. I., & Davis, J. H. (1994) *Biophys. J. 66*, 1415−1428.
Rose, M. E. (1957) *Elementary Theory of Angular Momentum*, Wiley, New York.
Separovic, F., Pax, R., & Cornell, B. A. (1993) *Mol. Phys. 78*, 357−369.
Teng, Q., Nicholson, L. K., & Cross, T. A. (1991) *J. Mol. Biol. 218*, 607−619.
Ulrich, A. S., Watts, A., Wallat, I., & Heyn, M. P. (1994) *Biochemistry 33*, 5370−5375.
Urry, D. W. (1971) *Proc. Natl. Acad. Sci. U.S.A. 68*, 672−676.
Urry, D. W., Walker, J. T., & Trapane, T. L. (1982) *J. Membr. Biol. 69*, 225−231.
Vega, S., & Pine, A. (1977) *J. Chem. Phys. 66*, 5624−5644.
Woolf, T. B., & Roux, B. (1994) *Proc. Natl. Acad. Sci. U.S.A.* (in press).
Woolf, T. B., Desharnais, J., & Roux, B. (1993) *NATO Advanced Workshop on Supramolecular Chemistry* (Wippf, G., Ed.) Kluwer, Dordrecht, The Netherlands.
Yeo, J. H., Demura, M., Asakura, T., Fujito, T., Imanari, M., Nicholson, L. K., & Cross, T. A. (1994) *Solid State NMR 3*, 209−218.

BI941494D